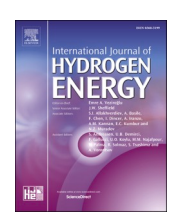
ELSEVIER

Contents lists available at ScienceDirect

International Journal of Hydrogen Energy

journal homepage: www.elsevier.com/locate/he



Insights from swirl number and ambient pressure variations with a hydrogen/ammonia swirl stabilized diffusion flame

Robin Vivoli 👵, Burak Goktepe, Daniel Pugh 👨, Steven Morris, Phil Bowen 💩, Agustin Valera-Medina 👨

Cardiff University, Cardiff, UK

ARTICLE INFO

Handling Editor: Mehran Rezaei

Keywords: Numerical modeling Swirl dynamics Hydrogen Ammonia Combustion

ABSTRACT

Contemporary research into decarbonized fuels such as H₂/NH₃ has highlighted complex challenges with applied combustion, with marked changes in thermochemical properties leading to significant issues such as limited operational range, flashback, and instability, particularly when attempts are made to optimize emissions production in conventional lean-premixed systems. Non-premixed configurations may address some of these issues but often lead to elevated NO_x production, particularly when ammonia is retained in the fuel mixture. Optimized fuel injection and blending strategies are essential to mitigate these challenges. This study investigates the application of a 75 %/25 %_{mol} H₂/NH₃ blend in a swirl-stabilized combustor, operated at elevated conditions of inlet temperature (500 K) and ambient pressure (0.11-0.6 MPa). A complex, nonmonotonic relationship between swirl number and increasing ambient combustor pressure is demonstrated, highlighting the intricate interplay between swirling flow structures and reaction kinetics, which remains poorly understood. At medium swirl (SN = 0.8) an increase in pressure initially reduces NO emissions, diminishing past ~ 0.3 MPa, with an opposing trend evident for high swirl (SN = 2.0) as NO emissions fall rapidly when combustor pressure approaches 0.6 MPa. High-fidelity numerical modeling is presented to elucidate these interactions in detail. Numerical data, generated using Detached Eddy Simulations (DES), were validated against experimental results to demonstrate a change in flame anchoring on the axial shear layer and marked change in recirculated flow structure, successfully capturing the features of higher swirl number flows. Favorable comparisons are made with optical data and a reduction in NO emissions with increasing pressure is demonstrated to replicate changes to the swirling flame chemical kinetics. Findings provide valuable insights into the combustion behavior of hydrogen-rich ammonia flames, contributing to the development of cleaner combustion technologies.

1. Introduction

Hydrogen is increasingly recognized as a key component to achieve decarbonized heat, power, and transport. However, there are operational challenges in delivery, flame stability and emissions production that influence the flexibility and performance of gas turbines, particularly in conventional dry-low emission systems [1]. While non-premixed combustors can enhance stability, NO_x production can increase, necessitating flexible control strategies. Recent studies [2–5] propose ammonia as a safe and efficient hydrogen carrier, that can be decomposed to form blends to mitigate reactivity/stability challenges.

Research into NH_3/H_2 fuels is increasing significantly, highlighting key strategies to influence kinetics and combustor performance [6,7]. For example, Valera-Medina et al. [8] found high NO_x emissions in a

50/50 vol% NH₃/H₂ mixture primarily due to excess OH and H radicals. Mashruk et al. [9] showed that increasing ammonia concentration from 50 % to 90 % in lean premixed NH₃/H₂ flames (Equivalence ratio, $\Phi=0.65$) results in lower NO and NO₂ emissions due to changes in relevant radicals, such as NH, OH, and NH₂. Similarly, Khateeb et al. [10] found that NO emissions in lean premixed NH₃ and H₂ flames ($\Phi=0.5$) are primarily influenced by Φ and NH₃ concentration rather than pressure. In contrast, Kim et al. [11] observed a reduction in OH and NO intensities with increasing pressure, which correlated with the upstream movement of the reaction zone and enhanced flame wrinkling. This aligns with other works demonstrating a reduction in NO emissions with an increase in ambient pressure for alternative combustor architectures and configurations [12–14].

Despite considerable research in swirl-stabilized systems, there is

E-mail address: vivolirc@cardiff.ac.uk (R. Vivoli).

^{*} Corresponding author.

limited information concerning the effects of recirculation and swirl number on these blends under elevated pressure conditions. This information is particularly important for swirl-stabilized diffusion flames commonplace in many gas turbine combustor architectures, as it can enhance flame stability and ensure mixture uniformity, thereby minimizing NO_{x} emissions, as highlighted by Okafor et al. [15]. Pugh et al. [16] identified a pronounced dependence of NO reduction on both pressure and swirl number (SN) when examining NO production pathways in various $\mathrm{NH}_3/\mathrm{H}_2$ blends within a non-premixed variable swirl burner.

In this context, it is essential to develop a comprehensive understanding of NH_3/H_2 combustion in swirl-stabilized diffusion flames under elevated conditions, which will ultimately increase its applicability in gas turbines.

1.1. Research aims

Previous work has demonstrated that at medium swirl increasing ambient pressure led to a sharp reduction in NO before plateauing, with the trend inverting for high swirl [16]. The aim of this study is to thoroughly investigate the complex relationship between swirl and flame thermochemistry for 75 $\%/25 \ \%_{mol} \ H_2/NH_3$ flames with pressure (0.11–0.6 MPa). The H_2/NH_3 ratio being selected to replicate highly cracked ammonia. Behaviors evident in the experimental data are further elucidated using Detached Eddy Simulations (DES), employing a modified reaction mechanism developed to visualize intermediate radicals prominent in NO formation chemistry. Work is performed in the context of emissions reduction for gas turbine applications, to assist in the development of cleaner and stable combustion technologies using well-established optical diagnostic techniques.

2. Materials and methods

2.1. Experimental and diagnostic setup

Experimental data were collected using a well-documented [12,13] geometrically generic swirl burner, designed and utilized at Cardiff University's Gas Turbine Research Center (GTRC).

2.1.1. Pressurized optical combustor

In this study the burner was setup in a non-premixed, co-annular flow configuration. A schematic of both the burner and pressure casing is presented in Fig. 1 with further detailed information on the setup available in other works [16].

Medium and high swirl nozzles were employed in this work with respective geometric swirl numbers equal to SN ≈ 0.8 and SN ≈ 2.0 as shown in Fig. 2(b) overleaf. Swirl was imparted only on the oxidizer stream, with fuel injected along the axial centerline immediately downstream of the swirler vanes. The geometric swirl number (Sg) was calculated as:

$$S_g = (A_{noz} \cdot r_{tan}) / (A_{tan} \cdot r_{noz}) \cdot (Q_{tan}/Q_{tot})^2$$

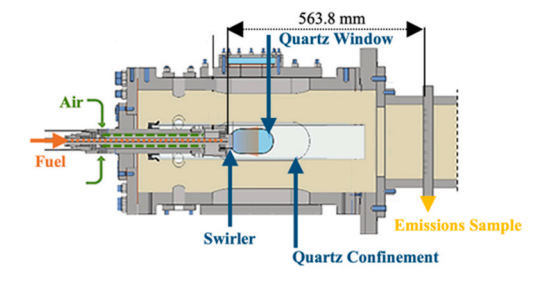


Fig. 1. Cross-sectional schematic of experimental burner and casing with emissions sampling probe location.

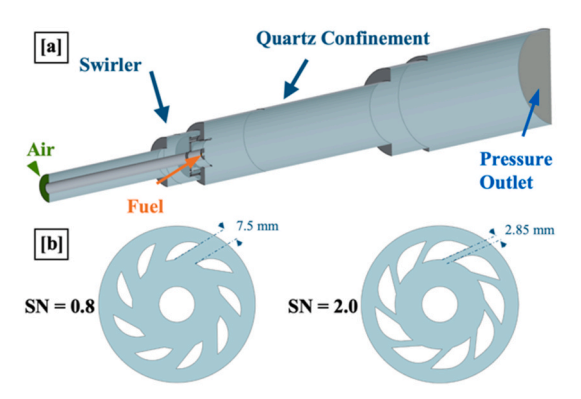


Fig. 2. Numerical burner domain [a] with comparison of swirler geometries employed for this work [b].

Where A_{noz} is the exit area of the burner exit nozzle, Atan is the area of the tangential inlet, r_{tan} is the effective radius of the tangential inlet, r_{noz} is the radius of the burner exit nozzle, Q_{tan} is the tangential flow rate, and Q_{tot} is the total flow rate.

2.1.2. Emissions measurement

Gaseous emissions were captured from the combustor exhaust, downstream of the quartz confinement using a nine-hole equal-area probe as per Pugh et al. [16]. NO emissions were normalized to a reference value of dry, 15 % O_2 in accordance with ISO 11042 [17]. Although it is recognized that this emission reporting method can overstate pollutant concentrations for high hydrogen content fuels when compared with hydrocarbons [18], the dry 15 % O_2 method was considered appropriate since this study does not focus on fuel switching.

Typical uncertainties of approximately ± 5 % of measurement account for analyzer specifications, linearization, and accuracy in span gas certification.

2.1.3. Chemiluminescence

Changes in flame structure were characterized via high-speed OH* chemiluminescence focusing on the well-known $A^2\Sigma^+ \to X^2\Pi$ OH* system [19]. Information on this high-speed imaging setup can be found in other works [12,16,20].

Chemiluminescence data were acquired at 4 kHz via a 315 nm (± 15 nm FWHM) narrow bandpass filter. Each dataset was temporally averaged over 2000 instantaneous images. The resulting averaged images were processed using a modified Abel inversion algorithm to generate a planar representation of the three-dimensional flame brush [12,16]. The Abel inversion assumes axisymmetry, which is an approximation in this study given the nine-bladed swirler geometry and the resulting slight flame asymmetry. To minimize associated uncertainty, the same side of the flame was consistently analyzed when presenting half-flame reconstructions. While this introduces a small deviation from perfect axisymmetry, the approach provides a reasonable representation of the global flame structure and allows meaningful comparison across conditions.

2.2. Numerical setup

Preliminary simulations employed Reynolds-Averaged Navier—Stokes (RANS) modeling, which accurately predicted NO reduction at elevated pressures for the SN0.8 cases but failed to capture the behavior of the SN2.0 cases, primarily due to insufficient turbulence resolution. To address this limitation, Spalart–Allmaras DES was implemented in STAR-CCM+ (version 2302). The DES framework applies Large Eddy Simulation (LES) in the core-flow regions and RANS in the near-wall regions, thereby enabling higher-fidelity predictions with substantially fewer computational cells compared to a full LES. The following

subsections detail the DES setup and validation. Due to the need for high-fidelity models, subsets of the experimental data representing the most extreme cases were chosen, as detailed in Section 2.2.3.

2.2.1. Geometry

The construction of the numerical domain is shown in Fig. 2(a), The combustion chamber and expansion sections were modeled to allow emissions sampling downstream of the burner face, aligning with the experimental configuration. Apart from physical differences between the mid (SN0.8) and high (SN2.0) swirlers, shown in Fig. 2(b), the domain remained unchanged, consistent with the experimental setup.

2.2.2. Meshing

To generate refined DES meshes, the integral length scale (L_0) , as defined in Eq. (1), was applied to preliminary RANS simulations, with adequate cell sizes established via Eq. (2) [21].

$$L_0 = k^{3/2} / \varepsilon \tag{1}$$

$$Aprox cell size = L_0/5 \tag{2}$$

Prism layers were applied to surfaces of interest with first cell heights varied across different faces to achieve an average $y^+\approx 1.$ The total height and number of prism layers was adjusted to ensure a smooth transition to the core mesh. The final DES meshes (Fig. 3) comprised ${\sim}16\times10^6$ and ${\sim}31\times10^6$ elements for the SN0.8 and SN2.0 cases respectively.

2.2.3. Physics setup and flows

A time-step of 1.25×10^{-5} s was chosen for all cases to maintain a Courant number (Co) of ~ 1 in the flame region. The time step was determined from preliminary RANS simulations by applying a field function of the reordered Co formulation, providing the time required for Co=1 within the flame region. Each time-step employed 20 inner iterations using the SIMPLEC segregated flow implicit scheme to aid convergence. Simulations ran for 2000 time-steps before initiating time-averaging which was performed for a maximum of 5000 time-steps.

The Otomo-2018 [22] reaction mechanism was utilized incorporating NH * and NH $_2^*$ species from Konnov [23,24], an approach equivalent to other works [25]. Segregated flow enthalpy was selected in conjunction with the Complex Chemistry model.

The fine mesh resolution needed to accurately capture both SN0.8 and SN2.0 domains using DES, coupled with the computational demands of Complex Chemistry and a species-rich reaction mechanism, resulted in highly resource-intensive simulations. As a result, even when utilizing 560 cores distributed over 14 nodes on the Hawk supercomputer, insufficient flow-through times were achieved to enable emissions measurement at the burner exhaust, in the equivalent location to where experimental measurements were taken. Instead, emissions data were sampled nearer to the flame, potentially leading to an offset in reported values. However, as discussed in Section 3.3, equivalent trends to the experimental results were observed, with the underlying mechanisms therefore representative. A reduced mechanism would ease computational burden at the potential expense of kinetic fidelity.

Inlet fuel and air mass flow rates, along with temperatures, were set to match experimental conditions, as summarized in Table 1 – note flow is scaled with pressure to maintain quasi-constant nozzle velocities (full

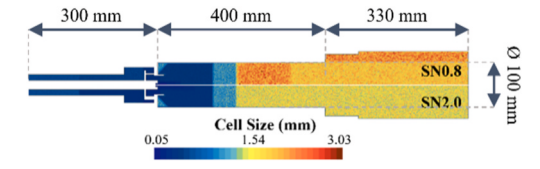


Fig. 3. SN0.8 [top] and SN2.0 [bottom] DES meshes.

Table 1
Mass flow and temperature inlet conditions for all simulations.

P _{Combustor} (MPa)	SN0.8		SN2.0	
	0.11	0.6	0.11	0.6
Fuel (g/s)	0.277	1.493	0.277	1.533
Air (g/s)	6.8	37.11	6.8	37.73
T _{Fuel} (K)	350			
T _{Air} (K)	500			

dataset available in supplemental material). Swirler nozzle and combustion wall temperatures were determined from thermocouple data collected during the experimental campaign.

Whilst both fuel and air inlet temperatures were maintained constant with pressure throughout the experimental campaign, the numerical fuel inlet temperature was prescribed as 350 K instead of the ambient delivery temperature of 300 K observed experimentally. This adjustment was based on heat transfer RANS simulations [26], which predicted fuel preheat of 50 K due to unavoidable thermal interaction with the heated airline, concentrically aligned with the fuel delivery line.

3. Results and discussion

3.1. Experimental data

Non-premixed NH $_3$ and H $_2$ /NH $_3$ flames have been observed to exhibit greater reductions in NO emissions with increasing pressure [12, 13,27]. This trend was previously confirmed by Pugh et al. [16]. Additionally, variations in swirl number were found to significantly influence NO reduction. A complex, non-monotonic relationship between swirl number and increasing ambient combustor pressure was demonstrated for the specified 75 %/25 % $_{\rm mol}$ H $_2$ /NH $_3$ mixture/condition, as illustrated in Fig. 4.

At medium swirl (SN = 0.8), Fig. 4 shows that increasing pressure initially reduces NO emissions, which then plateau beyond $\sim\!0.3$ MPa, with only minor variations thereafter. An opposing trend is evident for high swirl (SN = 2.0) as NO emissions fall rapidly when combustor pressure increases further. The greater radial momentum imparted by the high-swirl insert is therefore likely to play a significant role. At lower pressures, enhanced mixing may dominate, producing behavior more akin to a premixed system. At higher pressures, however, density-related effects may dampen the radial momentum, leading to more comparable performance between the two swirl inserts.

3.2. Numerical validation - flame behavior

Validation and investigations into the impact of pressure and SN on flame stabilization mechanisms and locations was performed against the experimental Abel transformed OH* chemiluminescence images captured 5 mm downstream of the nozzle exit over a 100×100 mm area. The colourmap for both numerical and experimental datasets was based on an image maximum normalization. For brevity, only half-flame profiles are presented, with the same half shown consistently for

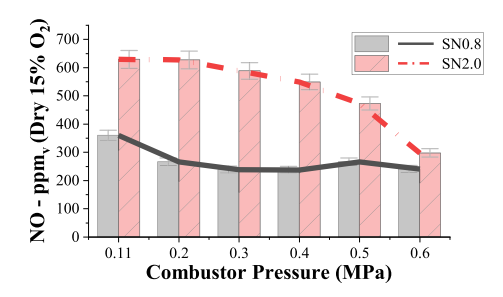


Fig. 4. Experimental changes in normalized NO with varying pressure and SN.

comparison. Results are collected in Fig. 5.

From Fig. 5, the numerical data can be seen to not exactly match the experimental results. This is expected, as the numerical data provides a direct cross-section of the flame, whereas the Abel-transformed data represents a reconstructed cross-section based on an axisymmetric assumption applied to line-of-sight integrated measurements [28].

Nevertheless, the numerical simulations successfully capture the changes in flame topology between SN0.8 and SN2.0, including the radial outward shift and flame thickening with increasing pressure. To further ascertain the numerical agreement with experimental flame shape variations in Fig. 5, the area of each half-flame exceeding a threshold of 0.4 was calculated. For the SN0.8 cases, numerical and experimental half-flames exhibited $\sim\!70$ % and $\sim\!72$ % increase in the area above this threshold with increasing pressure, respectively. Similarly, for SN2.0, numerical and experimental area increases were $\sim\!126$ % and $\sim\!175$ %, respectively. These results provide assurance that the numerical model suitably captures the observed experimental trends. Overall, the strong correlation between numerical and experimental data provides confidence for further investigations.

A key insight from the numerical results is the substantial shift in flame anchoring between the SN0.8 and SN2.0 cases. The 0-velocity isosurface overlay reveals that, in SN0.8 flames, anchoring occurs within the axial shear layer, whereas in SN2.0 flames, it shifts to the outer recirculation zone, aligning with the shear layer. This significant shift suggests changes in both the fuel consumption process and the location of NO formation, which will be examined in detail in Sections 3.3 and 3.4, respectively.

3.3. NO emissions

As previously described, numerical emissions data were collected by performing surface averages of a 100×100 mm constrained plane located 5 mm downstream of the nozzle tip. Although this approach does not allow for a direct comparison with the experimental data, the underlying trends can still be assessed. On average, the numerical inflame NO predictions were approximately 100 % higher than the experimental measurements when corrected to 15 % O_2 . This likely results from variance in the sampling location between numerical and experimental datasets (suggested from previous CRN modelling with NH₃/H₂ blends [13]) alongside other kinetic limitations specific to the reaction mechanism, and the effects of local heat loss [29].

Despite magnitude discrepancies, a strong overall correlation was present when examining relative changes as shown in Fig. 6 where both the numerical and experimental emissions datasets were normalized by their respective maximum values to enable direct comparison.

Fig. 6 shows that, for the SN0.8 cases, experimental and numerical results captured a $\sim\!33$ % and $\sim\!25$ % reduction in emissions respectively with increasing pressure. Swirler-induced variations at atmospheric

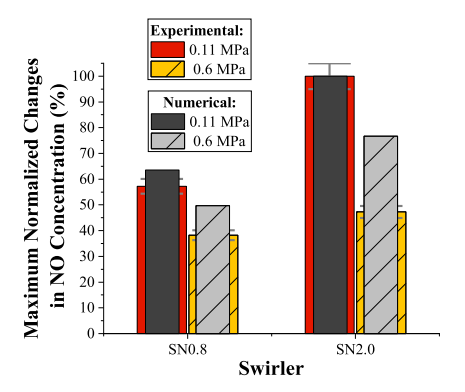


Fig. 6. Comparison of experimental (exhaust) and numerical (in-flame) NO emissions. Normalization based on the maximum in each SN dataset.

pressure also showed good agreement, with emissions increasing by $\sim\!75~\%$ experimentally and $\sim\!57~\%$ numerically when transitioning from SN0.8 to SN2.0. However, pressure-induced changes in the SN2.0 cases were less pronounced in the numerical results compared to the experimental data. The numerical results were consistent with experimental observations in indicating a stronger influence of pressure on NO reduction for SN2.0 compared with SN0.8. However, the experimentally measured reduction in emissions for SN2.0 relative to SN0.8 was approximately an order of magnitude greater than that predicted numerically.

Overall, the experimentally observed trends were replicated numerically, with some discrepancies noted for the 0.6 MPa SN2.0 case. Enhanced performance achieved through the DES simulations compared to RANS, suggests that LES may provide improved results.

3.4. Change in fuel burn

The concentrations of both H_2 and NH_3 within the swirler nozzle and combustion chamber were assessed by using surface-averaged section planes positioned perpendicular to the burner. These planes were axially spaced, extending from the nozzle exit (defined as the axial datum) both downstream into the combustion chamber (+ve) and upstream into the burner nozzle (-ve). Results for both swirlers, along with variations in the overall equivalence ratio (Φ) within the combustion chamber, are presented in Fig. 7.

From Fig. 7 it is evident that fuel consumption accelerates with increasing pressure across both swirlers, as also indicated by the enhanced heat release at higher pressures in Fig. 5. However, a notable difference in fuel concentrations within the swirler nozzle and combustion chamber is observed between the two swirlers. The increased swirl and enhanced mixing induced by SN2.0 result in higher $\rm H_2$ and

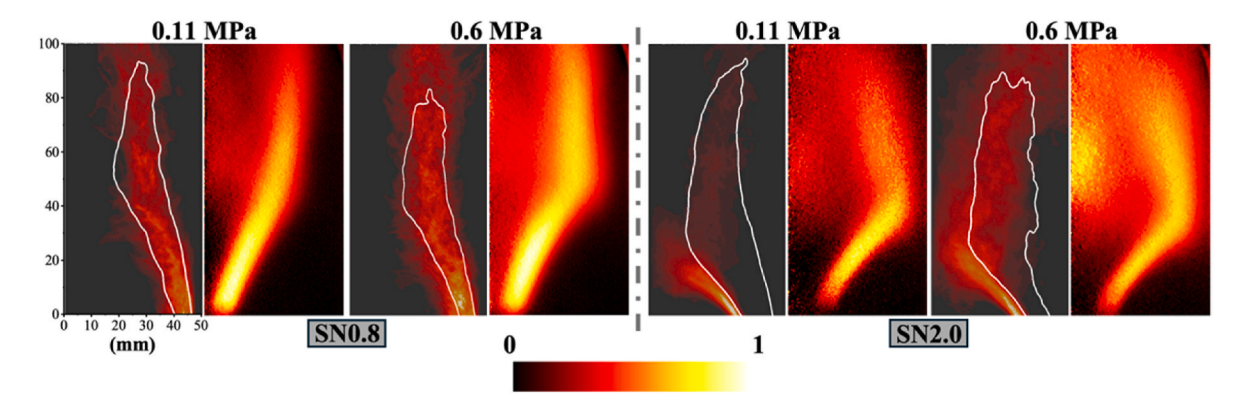


Fig. 5. For each condition: experimental Abel transformed OH* results [right] and numerical OH* values with white overlay of the 0-velocity iso-surface [left]. Colourmap normalized to image maximum for both experimental and numerical data.

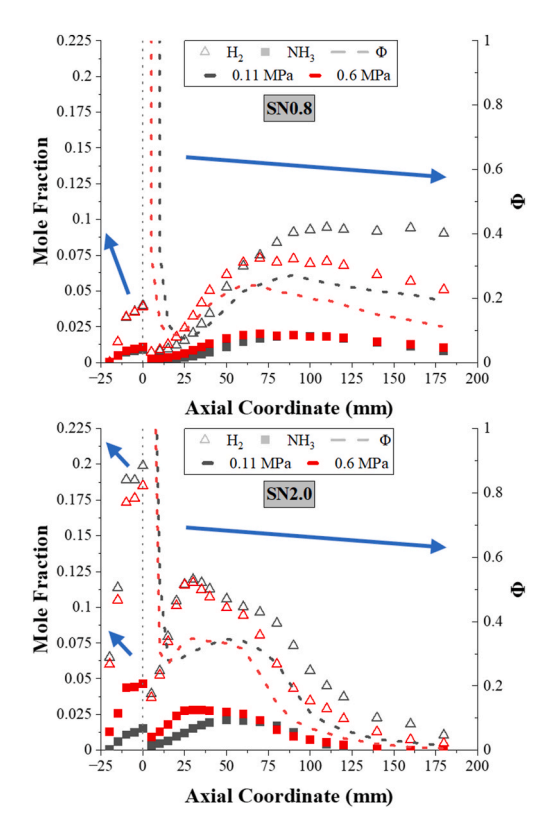


Fig. 7. Fuel concentration changes as both mole fractions and Φ at different surface-averaged axial points perpendicular to the burner. 0 corresponds to the nozzle tip.

 NH_3 concentrations within the swirler nozzle and the first ${\sim}50$ mm of the combustion chamber. Furthermore, fuel mole fractions within the combustion chamber exhibit a significantly steeper decline compared to the SN0.8 cases, a trend that will be further elucidated by examining Φ variations.

Both swirlers show a rapid Φ decline within the first 20 mm of the combustion chamber as the fuel jet loses momentum and mixes with the swirling air. Due to the stronger swirl induced by SN2.0, fuel-air mixing occurs earlier, with most fuel consumed beyond 150 mm from the nozzle exit. In contrast, SN0.8 cases retain fuel even 180 mm from the nozzle exit, with Φ values between 100 and 180 mm averaging $\sim\!4.3$ times higher than those in SN2.0 cases.

The greater fuel consumption facilitated by the flame anchoring in the outer recirculation zone, with improved mixing for SN2.0 supports the higher NO emissions observed for this swirler compared to SN0.8 at atmospheric pressure. However, since fuel is consumed even more rapidly at higher pressures, additional mechanisms must be responsible for the reduction in NO observed experimentally for the SN2.0 case at 0.6 MPa.

3.5. NO vs NH2*, NH* and OH*

The changes in flame anchoring with varying SN discussed in Section 3.2 underscored the necessity for further investigation into potential shifts in NO formation locations. Fig. 8 presents global-maximum normalized NO values captured 5 mm downstream of the nozzle exit over a 100×100 mm area, along with iso-surface overlays of global-maximum normalized NH₂*. NH₂* is selected as a representative marker for heat release with NH₃ flames [30], with ground state amidogen influential in NO chemistry [12,13]. For brevity, only half-flame profiles are shown, with the same half consistently displayed, and the 0.6 MPa cases vertically mirrored for easier comparison.

Fig. 8 illustrates a significant variation in peak NO formation

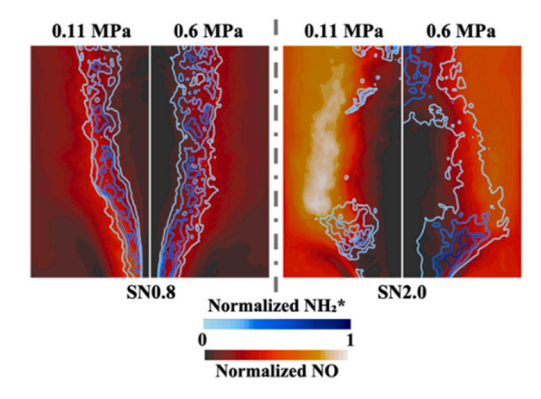


Fig. 8. Numerical molar NO with iso-surface overlay of NH2*. Both normalized based on the respective global maximus.

locations between the SN0.8 and SN2.0 cases. In the SN0.8 cases, NO is primarily generated within the inner recirculation zones, closely aligning with peak heat release regions observed in Fig. 5. Conversely, in the SN2.0 cases, peak NO production occurs outside the central recirculation zones, near the combustion chamber walls with little to no overlapping with peak heat release locations. This distinction implies notable differences in residence times, with the SN0.8 cases exhibiting longer NO residence due to its presence within the central recirculation zones.

NH₂ is recognized as being crucial for enhancing NO consumption through the chain-carrying reaction NH₂+NO \leftrightarrow NNH + OH, and the terminating reaction NH₂+NO \leftrightarrow H₂O + N₂ [13]. OH and O are also important for the oxidation of NH and NH₂ to NO via HNO and the reaction HNO + OH \leftrightarrow NO + H₂O [31]. A positive correlation between ground state and excited species [12] suggests that the increase in NH₂* and reduction in regions of OH*, both analyzed in this study, contribute to a decrease in NO concentrations. As shown in the NH₂* overlays in Fig. 8, higher molar concentrations of NH₂* were recorded for the SN2.0 case at 0.6 MPa, with a significant increase compared to the atmospheric case. In contrast, for the SN0.8 cases, little change in NH₂* concentration was observed as pressure increased.

A more quantitative assessment of NH₂*, NH*, and OH* molar concentrations was conducted by averaging their values within a constrained 100 \times 100 mm combustion chamber section, positioned 5 mm downstream of the burner exit. Pressure-induced percentage changes relative to the 0.11 MPa cases for each swirler are collected in Fig. 9.

From Fig. 9, pressure-induced changes in OH* fractions can be seen to be consistent across both swirlers with reductions of $\sim\!80$ % for SN0.8 and $\sim\!72$ % for SN2.0 as pressure increased from 0.11 to 0.6 MPa. In contrast, NH₂* and NH* exhibited order-of-magnitude increases for SN2.0 compared to SN0.8. Specifically, for SN0.8, NH* saw no pressure sensitivity and NH₂* increased by $\sim\!17$ %. For SN2.0 however, NH* and NH₂* molar concentrations increased by $\sim\!102$ % and 170 %, respectively, under elevated pressure conditions.

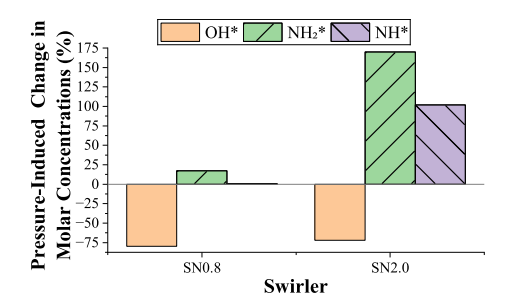


Fig. 9. Pressure-induced percentage changes in in-flame molar concentration of OH^* , NH_2^* and NH^* normalized against atmospheric values for each swirler dataset.

Overall, consistent with Kim et al. [11], at SN=2.0 we observe a reduction in OH^* and NO with increasing pressure, whereas at SN=0.8 the NO response is comparatively weak, in line with the pressure-insensitive behavior reported by Khateeb et al. [10]. These findings demonstrate that swirl intensity plays a crucial role in determining NO formation locations and excited species distributions. Additionally, the significant increase in NH_2^* and NH^* concentrations at elevated pressure for SN2.0, contrasted with minimal changes for SN0.8, suggests an enhanced role of NH_2 -mediated NO reduction in high-swirl conditions at elevated pressures, particularly in the outer recirculating flow.

4. Conclusions

This study presents an experimental and numerical investigation of swirl number on flame stabilization and pressure-induced changes in NO production pathways, in a non-premixed variable swirl burner with 75 $\%/25~\%_{mol}~H_2/NH_3$ flames. These numerical results provide insight into the mechanisms behind pressure-dependent NO production differences, particularly at high swirl, as observed experimentally. The model successfully captured the overall trends in flame shape and NO reduction.

The main conclusions are as follows.

- Change from medium (SN0.8) to high (SN2.0) swirl provided a change in flame anchoring location, providing a marked change in emissions production.
- Significant changes in fuel concentrations were observed between the swirlers. SN2.0 induced faster fuel consumption due to enhanced mixing, leading to higher $\rm H_2$ and $\rm NH_3$ concentrations within the swirler nozzle and the first ~ 50 mm of the combustion chamber. This resulted in a steeper decline in fuel fractions in the combustion chamber compared to SN0.8, quantifying the influence of swirl intensity on fuel consumption.
- A marked difference in both peak NO and OH* formation locations
 was observed between SN0.8 and SN2.0. In SN0.8 cases, OH* formation and peak heat release concentrated along the inner shear
 layer, whereas in SN2.0, it shifted outward, aligning with the outer
 recirculation zone. In SN0.8, NO formed within the inner recirculation zones, while in SN2.0, peak NO production occurred in the outer
 flow regions, near the combustion chamber walls.
- Pressure increased NH₂* and NH* concentrations by an order of magnitude for SN2.0, while OH* concentrations showed similar reductions for both swirlers. This indicates a stronger role of NH₂mediated NO reduction under high-swirl, high-pressure conditions, leading to enhanced NO consumption in the outer flow.

CRediT authorship contribution statement

Robin Vivoli: Writing – original draft, Methodology, Data curation. Burak Goktepe: Writing – review & editing, Data curation. Daniel Pugh: Writing – review & editing, Funding acquisition, Conceptualization. Steven Morris: Writing – review & editing, Investigation. Phil Bowen: Writing – review & editing. Agustin Valera-Medina: Writing – review & editing, Funding acquisition, Conceptualization.

Declaration of competing interest

The authors declare that they have no known competing financial interests or personal relationships that could have appeared to influence the work reported in this paper.

Acknowledgements

This work was supported by the Engineering and Physical Sciences Research Council (EPSRC), Cardiff School of Engineering through the Centre for Doctoral Training in Resilient Decarbonized Fuel Energy Systems [Grant Number EP/S022996/1]; FLEXnCONFU; and the

Supercomputing Wales project, which is part-funded by the European Regional Development Fund (ERDF) via Welsh Government. For the purpose of open access, the author has applied a CC BY copyright license to any Author Accepted Manuscript version arising. Information on the data underpinning this publication, including access details, can be found in the Cardiff University Research Data Repository at [10.17035/cardiff.29987587].

References

- [1] Taamallah S, Vogiatzaki K, Alzahrani FM, Mokheimer EMA, Habib MA, Ghoniem AF. Fuel flexibility, stability and emissions in premixed hydrogen-rich gas turbine combustion: technology, fundamentals, and numerical simulations. Appl Energy 2015;154:1020–47. https://doi.org/10.1016/j.apenergy.2015.04.044.
- [2] Lee JH, Lee SI, Kwon OC. Effects of ammonia substitution on hydrogen/air flame propagation and emissions. Int J Hydrogen Energy 2010;35:11332–41. https://doi. org/10.1016/j.ijhydene.2010.07.104.
- [3] Joo JM, Lee S, Kwon OC. Effects of ammonia substitution on combustion stability limits and NOx emissions of premixed hydrogen–air flames. Int J Hydrogen Energy 2012;37:6933–41. https://doi.org/10.1016/j.ijhydene.2012.01.059.
- [4] Um DH, Joo JM, Lee S, Kwon OC. Combustion stability limits and NOx emissions of nonpremixed ammonia-substituted hydrogen—air flames. Int J Hydrogen Energy 2013;38:14854–65. https://doi.org/10.1016/j.ijhydene.2013.08.140.
- [5] Pashchenko D. Ammonia fired gas turbines: recent advances and future perspectives. Energy 2024;290:130275. https://doi.org/10.1016/j. perspectives. 2024.19235
- [6] Mazzotta L, Meloni R, Lamioni R, Romano C, Galletti C, Borello D. Numerical investigation of NOx emissions in a gas turbine burner using hydrogen-ammonia and partially cracked ammonia fuel blends: a combined LES and CRN approach. Appl Therm Eng 2025;278:127330. https://doi.org/10.1016/j. applthermaleng.2025.127330.
- [7] Kumuk O, Ilbas M. Comparative analysis of ammonia/hydrogen fuel blends combustion in a high swirl gas turbine combustor with different cooling angles. Int J Hydrogen Energy 2024;52:1404–18. https://doi.org/10.1016/j. iihydene.2023.07.166.
- [8] Valera-Medina A, Pugh DG, Marsh P, Bulat G, Bowen P. Preliminary study on lean premixed combustion of ammonia-hydrogen for swirling gas turbine combustors. Int J Hydrogen Energy 2017;42:24495–503. https://doi.org/10.1016/j. ijhydene.2017.08.028.
- [9] Mashruk S, Okafor EC, Kovaleva M, Alnasif A, Pugh D, Hayakawa A, et al. Evolution of N2O production at lean combustion condition in NH3/H2/air premixed swirling flames. Combust Flame 2022;244:112299. https://doi.org/ 10.1016/j.combustflame.2022.112299.
- [10] Khateeb AA, Guiberti TF, Wang G, Boyette WR, Younes M, Jamal A, et al. Stability limits and NO emissions of premixed swirl ammonia-air flames enriched with hydrogen or methane at elevated pressures. Int J Hydrogen Energy 2021;46: 11969–81. https://doi.org/10.1016/j.jihydene.2021.01.036.
- [11] Kim JH, Kim TW, Kim YH, Kwon OC. Combustion characteristics of premixed ammonia-hydrogen/air swirl flames at elevated pressure. Int J Hydrogen Energy 2024;74:423–33. https://doi.org/10.1016/j.ijhydene.2024.06.134.
- [12] Pugh D, Runyon J, Bowen P, Giles A, Valera-Medina A, Marsh R, et al. An investigation of ammonia primary flame combustor concepts for emissions reduction with OH*, NH2* and NH* chemiluminescence at elevated conditions. Proc Combust Inst 2021;38:6451–9. https://doi.org/10.1016/j.proci.2020.06.310.
- [13] Pugh D, Bowen P, Valera-Medina A, Giles A, Runyon J, Marsh R. Influence of steam addition and elevated ambient conditions on NOx reduction in a staged premixed swirling NH3/H2 flame. Proc Combust Inst 2019;37:5401–9. https://doi.org/ 10.1016/j.proci.2018.07.091.
- [14] Somarathne KDKA, Hatakeyama S, Hayakawa A, Kobayashi H. Numerical study of a low emission gas turbine like combustor for turbulent ammonia/air premixed swirl flames with a secondary air injection at high pressure. Int J Hydrogen Energy 2017;42:27388–99. https://doi.org/10.1016/j.ijhydene.2017.09.089.
- [15] Okafor EC, Somarathne KDKA, Hayakawa A, Kudo T, Kurata O, Iki N, et al. Towards the development of an efficient low-NOx ammonia combustor for a micro gas turbine. Proc Combust Inst 2019;37:4597–606. https://doi.org/10.1016/j. proci.2018.07.083.
- [16] Pugh D, Bowen P, Navaratne R, Goktepe B, Giles A, Valera Medina A, et al. Influence of variable swirl on emissions in a non-premixed fuel-flexible burner at elevated ambient conditions. J Eng Gas Turbines Power 2024;146. https://doi.org/ 10.1115/1.4063786.
- [17] British Standard. ISO 11042-1:1996 gas turbines exhaust gas emission measurement and evaluation. UK, 1996.
- [18] Douglas CM, Shaw SL, Martz TD, Steele RC, Noble DR, Emerson BL, et al. Pollutant emissions reporting and performance considerations for hydrogen-hydrocarbon fuels in gas turbines. J Eng Gas Turbines Power 2022;144. https://doi.org/ 10.1115/1.4054949.
- [19] Gaydon AG. The spectroscopy of flames. second ed. Netherlands: Springer Netherlands; 1974.
- [20] Runyon J, Giles A, Marsh R, Pugh D, Goktepe B, Bowen P, et al. Characterization of additive layer manufacturing swirl burner surface roughness and its effects on flame stability using high-speed diagnostics. J Eng Gas Turbines Power 2020;142. https://doi.org/10.1115/1.4044950.

- [21] Basu S, DeMarco AW, He P. On the dissipation rate of temperature fluctuations in stably stratified flows. https://doi.org/10.1007/s10652-020-09761-7; 2020.
- [22] Otomo J, Koshi M, Mitsumori T, Iwasaki H, Yamada K. Chemical kinetic modeling of ammonia oxidation with improved reaction mechanism for ammonia/air and ammonia/hydrogen/air combustion. Int J Hydrogen Energy 2018;43:3004–14. https://doi.org/10.1016/j.ijhydene.2017.12.066.
- [23] Konnov AA. An exploratory modelling study of chemiluminescence in ammonia-fuelled flames. Part 1. Combust Flame 2023;253:112788. https://doi.org/10.1016/j.combustflame.2023.112788.
- [24] Konnov AA. An exploratory modelling study of chemiluminescence in ammonia-fuelled flames. Part 2. Combust Flame 2023;253:112789. https://doi.org/10.1016/j.combustflame.2023.112789.
- [25] Panoutsos C, Hardalupas Y, Taylor A. Numerical evaluation of equivalence ratio measurement using OH* and CH* chemiluminescence in premixed and nonpremixed methane–air flames. Combust Flame 2009;156:273–91. https://doi.org/ 10.1016/j.combustflame.2008.11.008.
- [26] Shahi M, Kok JBW, Roman Casado JC, Pozarlik AK. Transient heat transfer between a turbulent lean partially premixed flame in limit cycle oscillation and the

- walls of a can type combustor. Appl Therm Eng 2015;81:128–39. https://doi.org/10.1016/j.applthermaleng.2015.01.060.
- [27] Hayakawa A, Goto T, Mimoto R, Arakawa Y, Kudo T, Kobayashi H. Laminar burning velocity and markstein length of ammonia/air premixed flames at various pressures. Fuel 2015;159:98–106. https://doi.org/10.1016/j.fuel.2015.06.070.
- [28] Schmidt BE, Page WE, Sutton JA. On the application of the abel transformation in statistically axisymmetric turbulent flows. AIAA J 2022;60:2169–77. https://doi. org/10.2514/1.J060819.
- [29] Davies J, Mazzotta L, Sato D, Mashruk S, Pugh D, Borello D, et al. Experimental and numerical investigation of NH3/H2/N2 combustion in a premixed/stratified swirl burner. J Eng Gas Turbines Power 2025;147. https://doi.org/10.1115/1.4066207.
- [30] Karan A, Khan-Ghauri M, Grégoire CM, Mathieu O, Petersen EL, Dayma G, et al. Detailed study of NH2* chemiluminescence in ammonia combustion. In: 2nd symposium on ammonia energy; 2023. Orléans, France.
- [31] Kobayashi H, Hayakawa A, Somarathne KDKA, Okafor EC. Science and technology of ammonia combustion. Proc Combust Inst 2019;37:109–33. https://doi.org/ 10.1016/j.proci.2018.09.029.